The effect of the carboxylation degree on cellulose nanofibers and waterborne polyurethane/cellulose nanofiber nanocomposites properties

Izaskun Larraza [a], Julen Vadillo [a,b], Arantzazu Santamaria-Echart [a], Alvaro Tejado [c], Maider Azpeitia [c], Eneritz Vesga [c], Ander Orue [a], Ainara Saralegi [a], Aitor Arbelaiz [a,], Arantxa Eceiza [a]

[a] '*Materials and Technologies*' *Research Group (GMT), Department of Chemical and Environmental Engineering, Faculty of Engineering of Gipuzkoa,*

University of the Basque Country, Pza Europa 1, Donostia-San Sebastian, 20018, Spain

[b] *IPREM - Equipe de Physique et Chimie des Polym`eres, UMR CNRS 5254, Universit´e de Pau et des Pays de l'Adour, H´elioparc 2, av. Pdt Angot, 64053, Pau cedex, 09, France*

[c] *Sustainable Construction Division, TECNALIA, A´rea Anardi 5, 20730, Azpeitia, Spain*

Abstract

There has been an exponential rise in the interest for waterborne polyurethanes (WBPU), due to the easy customizability of their properties and their ecofriendly nature. Moreover, their aqueous state facilitates the incorporation of hydrophilic reinforcements. Cellulose nanofibers (CNFs) have shown great potential, thanks to their renewability, large natural availability, low cost and great specific properties. However, CNFs often require some modification to obtain optimal compatibility. In this work, standard bleached hardwood kraft pulp has been subjected to a carboxylation process followed by mechanical disintegration. Varying treatment times and passes, CNF samples with different carboxylation degrees have been obtained. WBPU/CNF nanocomposites with different CNF content have been prepared. The effect of the carboxylation degree on the CNFs and on the nanocomposites properties has been studied. Although carboxylation damaged the cellulose structure, decreasing the crystallinity degree of CNF and reducing the thermal stability of fibers, composites showed better thermal and thermomechanical stability and improved mechanical properties than the unreinforced matrix counterpart. A maximum increase of 1670% in modulus, 377% in stress at yield and 86% in stress at break has been achieved for composites reinforced with carboxylated fibers. Therefore, it was observed that carboxylation improved matrix/ reinforcement interactions.

Keywords: Cellulose; Nanocomposite; Fibre/matrix bond; Mechanical properties

1. Introduction

The increasing awareness of environmental issues and the subsequent stricter legislations for emissions have skyrocketed the interest in replacing conventional materials with more environmentally friendly ones [1]. Among them, water-based polymeric dispersions have gained great interest, due to their lack of volatile organic compound emissions and the remarkable potential shown for many applications [2,3]. It is well-known that polyurethane- based materials (elastomers, adhesives, coatings, foams, etc.) are a key component of the plastic industry, being in the year 2015 the fifth among the most produced polymers in Europe [4] and seventh worldwide [5]. Therefore, the demand for water-based poly- urethane dispersions is growing rapidly in the plastic industry. The wide range of customizable properties, depending on reagent chemical structure, molar ratio and synthesis procedure, open the door to specifically designed polyurethane-based materials, very beneficial in numerous applications [6]. Polyurethanes are block copolymers usually formed by two incompatible segments providing different properties, a soft segment (SS) composed by a macrodiol, and a hard segment (HS) consisting on an isocyanate and a low molecular weight diol or diamine. Thus, properties can be easily tailored by varying segment ratios [7]. Moreover, in recent years, sustainability has become a major concern when

designing materials. Finding new bio-sourced monomers for plastics is a key factor for the transition towards more environmentally friendly materials. Precursors obtained from renewable sources, mainly vegetable oils, can be used in the synthesis of water-based (waterborne) polyurethane dispersions, such as polyols from castor oil [8] and soybean oil [9], and fatty acid-derived isocyanates [10,11].

There is abundant literature referred to the addition of different reinforcements to waterborne polyurethane dispersions: clay, silica, silver, graphene [12], among others. In this field, the use of nanocellulose has gained great interest in the last years due to its great specific mechanical and chemical properties, low density, as well as biodegradability, biocompatibility and natural availability, promoting also to the development of sustainable materials [13,14].

Nonetheless, depending on the nature of the polymeric matrix, nanocellulose can be either incorporated into composites directly without modification in polar matrices, such as polyvinyl alcohol [15,16], or after being subjected to some sort of derivatization [14,17,18], when hydrophobic matrices are used, to avoid agglomeration of nanocellulose particles in the polymeric matrix. Modification of the nanocellulose surface with chemical groups has been extensively studied [17,19,20]. The most common chemical routes are based on chemical reactions or interactions through the numerous and highly reactive hydroxyl groups available on nanocellulose surface. The oxidation of OH groups into carboxylic moieties has been extensively performed as a successful strategy to decrease the energy consumption when isolating cellulose nanofibers (CNFs) from cellulose fibers. TEMPO-mediated oxidation [21] method is the most extensively studied method for the oxidation of the primary OH groups. However, it is also possible to achieve carboxylation through the secondary OH groups by sequential periodate-chlorite oxidation [22].

Studies analyzing the effect of the carboxylation degree on cellulose nanoentities have shown changes in properties, such as crystallinity, surface area and cell viability [23,24]. When preparing composites with oxidized fibers, most works study the effect of the modification [25], but to the best of our knowledge there are no works that focus on the effect of the carboxylation degree on the final composites properties.

This work aims to study both the effect of carboxylation and its degree on nanocellulose properties as well as on composite properties. For that, CNFs with different carboxylation degrees have been achieved through the less studied oxidation of the secondary OH groups. CNFs have been used as reinforcement for a waterborne polyurethane matrix synthesized with a polyol coming from renewable sources. Finally, composite with different amounts of CNFs and with different grades of carboxylation have been prepared and analyzed.

To better study both the carboxylation and the carboxylation degree effects, first the modified and pristine CNFs have been deeply characterized, in order to not only consider the effect of oxidized groups, but also the resultant changes in crystallinity, thermal stability and morphology of the fibers, among others.

On the one hand, it is expected that the hydrophilic nature of both WBPU and CNFs will facilitate the miscibility of the systems and thereby improve the mechanical properties of the final composites. On the other hand, the oxidation of CNF hydroxyl groups could improve the compatibility between CNFs and WBPU matrix and result in significantly altered composite properties. The different CNFs systems and the prepared WBPU-CNF nanocomposite films have been analyzed using different characterization techniques.

2. Experimental

2.1. Materials

For the synthesis of the waterborne polyurethane, a difunctional polyol coming from renewable sources, Priplast 3192® (M_w 2000 g mol^{-1}), purchased from Croda, has been used as soft segment. Isophorone diisocyanate (IPDI), kindly supplied from Covestro, 2,2- Bis (hydroxymethyl) propionic acid (DMPA), used as internal emulsifier, provided from Aldrich and ethylene diamine (EDA), as chain extender, provided from Fluka, were used as hard segment. Triethylamine (TEA), provided by Fluka, was employed to neutralize the carboxylic groups of DMPA, and dibutyltin dilaurate (DBTDL), provided from Aldrich, was used as catalyst. Both the polyol and the DMPA were dried under vacuum at 60 °C for 4 h prior to their use. Standard bleached hardwood kraft pulp (bHKP) from *Eucalyptus globulus*, obtained from a local paper mill, was used as raw material for the preparation of CNFs. Sodium metaperiodate ($NaIO_4$), sodium chloride (NaCl), hydrogen peroxide (H_2O_2), sodium hydroxide (NaOH) and sodium chlorite ($NaClO_2$), used for the cellulose treatment, were purchased from Scharlab and used as received.

2.2. Preparation of cellulose nanofibers

Initially, bHKP sheets were torn into ca. 2-4 cm^2 pieces and soaked in tap water for 24 h to allow complete swelling. The mixture was then dispersed mechanically until no agglomeration of fibers could be observed, and final consistency was then adjusted to 1 wt%. A reference CNF sample (CNF0) was obtained directly from this pulp suspension by subjecting it to 10 passes through a Masuko Supermass Colloider (MKZA10-15J), after which no microstructure could be seen under an optical microscope.

In parallel, the pulp suspension was subjected to a sequential periodate-chlorite oxidation as described elsewhere [22,26]. Briefly, a 500 g deionized water suspension containing 5 g of cellulose fibers, 3.33 g of sodium metaperiodate (50% molar ratio of cellulose anhydroglucopyranose units, 0.03 M overall concentration) and 14.5 g of NaCl (0.75 M) was allowed to react under total darkness and agitation for alternatively 2 and 24 h, in order to prepare CNFs with different carboxylation degrees. After that time, the reacted mixture was washed four times with deionized water and used as starting material for the second oxidation reaction. In this second reaction, a new 500 g deionized water suspension was prepared with 5 g of dialdehyde cellulose fibers resulting from the previous step together with 3.5 g of $NaClO_2$ (0.04 M concentration), 14.5 g of NaCl (0.75 M) and 3.3 g of H_2O_2. This mixture was allowed to react for 2 h at room temperature. During this time, the pH of the suspension was maintained between 4.2 and 4.5 by dropwise addition of NaOH 0.5 N. The slight excess of chlorite is expected to fully convert aldehyde groups introduced by periodate into carboxylic groups with the aid of the co-oxidant hydrogen peroxide. In both oxidation reactions, the presence of sodium chloride increases the ionic strength of the medium boosting up the efficiency of the reactions due to the decrease of the electrical double layer [27]. Finally, the reaction mixture was filtered and the dicarboxylated cellulose fibers washed repeatedly.

The carboxylic cellulose preparations were fully disintegrated in the Masuko Supermass Colloider until no presence of the fiber wall could be found under the optical microscope, what happened only after 8 (for CNF1) and 3 (for CNF2) passes due to the strong effect of carboxylate groups on fibrillation (via repulsive forces). After that point, the application of new passes on the suspension produces no increase on the degree of fibrillation of the fibers, which are already totally converted into nanoentities. Table 1 resumes the name and characteristics of the three CNF preparations. The cellulose nanofibers with three different carboxylation degrees were named as CNF0, CNF1 and CNF2.

2.3. Preparation of waterborne polyurethanes (WBPU)

The synthesis of the WBPU was carried out using a two-step polymerization procedure in a 250 mL four-necked flask equipped with a mechanical stirrer, thermometer and nitrogen inlet within a thermostatic bath. In the first step the prepolymer, composed by the polyol and the diisocyanate, was synthesized and in the second step the chain extension was carried out. The reaction progress was monitored using the dibutylamine back titration method according to ASTM D 2572-97. In the first step of the reaction, polyol, IPDI and 0.037 wt% of DBTL respect to the prepolymer content were reacted at 100 °C for 5 h under mechanical stirring, then the DMPA neutralized with TEA and dissolved in a little amount of acetone was added at 50 °C and left to react for 1 h more. The system was then cooled down to room temperature, where the phase inversion step was carried out by dropwise addition of deionized water under vigorous stirring. Finally, in the second step of the synthesis, the chain extender (EDA) was added at room temperature and the mixture was allowed to react for 2h at 35 °C under stirring, forming a water dispersion with a solid content of 31 wt%. The resulting molar ratio of polyol/DMPA/IPDI/EDA was 1/1.1/3.5/0.6.

Table 1. Characteristics of the CNF preparations used in this study.

	Name		
Treatment	**CNF0**	**CNF1**	**CNF2**
IO_4 oxidation time (h)	–	2	24
ClO_2 oxidation time (h)	–	2	2
#Passes Masuko	10	8	3

2.4. Preparation of WBPU-CNF composites

Nanocomposite films based on WBPU and CNF were prepared by solvent casting method. Nanocellulose aqueous suspensions were sonicated at room temperature for 1 h and, after addition of WBPU, the mixtures were sonicated for 1 h more. 45 mL samples of these mixtures were prepared, adjusting the total volume with extra addition of water in those cases of low nanocellulose content. Samples were casted in Teflon molds and dried first at room temperature for 7 days, and then under vacuum at 25 °C for 3 days. Films with a thickness around 0.4 mm containing 1.5, 3 and 5 wt% of nanocellulose were prepared. Nanocomposites were named as “x CNFy”, where “x” denotes nanocellulose wt% respect to the total mass of the composite and “y” the nanocellulose type used in the composite.

2.5. Characterization

2.5.1. Scanning electron microscopy (SEM)

The morphology of the nanofibers was analyzed via electron scanning microscopy using a JSM-6400 scanning microscope working at a 7 mm distance to the mat and 20 kV. Samples were coated (Quorum Q150TES) with a 20 nm gold coat in order to make them conductors. Nanofiber dimensions were measured from these images via ImageJ software.

Morphology of the composites was also studied through scanning electron microscopy. Images were obtained with a FEI ESEM Quanta 200, operating at 5–20 kV. In order to prepare samples, they were first frozen in liquid nitrogen and a cryofracture of the cross-section was done. Samples were held with a clamp and the analyses took place under vacuum.

2.5.2. X-ray crystallography (XRD)

X-ray powder diffraction patterns were collected by using a Philips X'pert PRO automatic diffractometer operating at 40 kV and 40 mA, in theta-theta configuration, a secondary monochromator with Cu-Kα radiation (λ = 1.5418 Å) and a PIXcel solid state detector (active length in 2θ 3.347°). Data were collected from 5 to 75° 2θ (step size 0.026 and time per step 80 s) at room temperature. A fixed divergence and antiscattering slit giving a constant volume of sample illumination were used.

2.5.3. Dynamic light scattering (DLS)

The particle size of the WBPU dispersion and its distribution was measured by dynamic light scattering, using a BI-200SM goniometer from Brookhaven. The intensity of dispersed light was measured using a luminous source of He–Ne laser (Mini L-30, wavelength 637 nm, 400 mW) and a detector (BI–APD) placed on a rotary arm which allows measuring the intensity at 90°. Samples were prepared mixing a small amount of aqueous dispersion with ultrapure water and measurements were carried out at 25 °C by triplicate every 2 months during half a year to ensure the stability of the dispersions.

2.5.4. Fourier transform infrared spectroscopy (FTIR)

The characteristic functional groups of nanocelluloses, WBPU and the composites were analyzed by Fourier transform infrared spectroscopy using a Nicolet Nexus spectrometer provided with a MKII Golden Gate accessory (Specac) with a diamond crystal at a nominal incidence angle of 45° and ZnSe lens. Spectra were recorded in attenuated reflection (ATR) mode between 4000 and 650 cm^{-1} averaging 32 scans with a resolution of 4 cm^{-1}.

2.5.5. Thermogravimetric analysis (TGA)

The thermal stability of WBPU, the different nanocelluloses and the composites were determined by thermogravimetric analysis (TGA) performed in a TGA/STDA 851 (Mettler Toledo) equipment. The samples were heated from 30 to 700 °C in a nitrogen atmosphere at a scanning rate of 10 °C min^{-1}.

2.5.6. Differential scanning calorimetry (DSC)

The thermal properties of the composites were determined by differential scanning calorimetry using a Mettler Toledo DSC 3^{+} equipment provided with a robotic arm and an electric intracooler as refrigerator unit. Between 5 and 10 mg of sample were encapsulated in aluminum pans and heated from −65 to 200 °C at a scanning rate of 10 °C min^{-1} in nitrogen atmosphere. From the heating thermograms, order-disorder transition temperature and enthalpy, as the maximum of the peak and the area below the peak, respectively, as well as glass transition temperature, as the inflection point of the curve, were determined.

2.5.7. Dynamic mechanical analysis (DMA)

The viscoelastic behavior of the films was determined by dynamic mechanical analysis using an Eplexor 100 N analyzer Gabo equipment. The measurements were carried out in tensile mode from −100 to 180 °C at a scanning rate of 2 °C min^{-1}. The initial strain was established as 0.05% and the operating frequency was fixed at 1 Hz.

2.5.8. Mechanical testing

Mechanical tests were performed in an Instron 5967 testing machine provided with a 500 N load cell and pneumatic grips to hold the samples. Samples were cut (2.8 mm in width and 0.4 mm in thickness) and tested at a crosshead speed of 20 mm min^{-1} at room temperature with a distance between clamps of 10 mm. Tensile modulus (E), stress at yield (σ_y), stress at break (σ_b) and

elongation at break (ε_b) were determined from stress-strain curves of five specimens of each series.

3. Results and discussion

3.1. Cellulose nanofibers characterization

The scanning electron microscopy images of the nanofibers are shown in Fig. 1. As can be observed, the applied chemical and mechanical treatments result in a network of nanofibers of 15–40 nm in diameter and several micrometers in length.

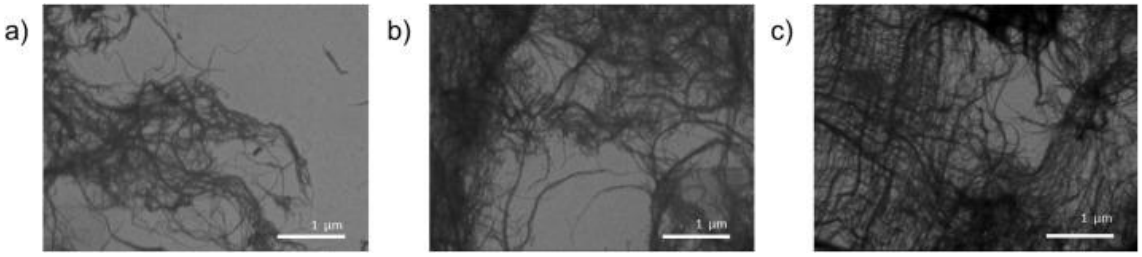

Fig.1. SEM images of cellulose nanofibers with different carboxylation degrees: a) CNF0, b) CNF1 and c) CNF2.

The carboxyl group concentration or carboxylation degree of all nanocelluloses was measured via conductometric titration as described elsewhere [22,26]. The results show an increase in carboxylation degree, going from 0.14 mmol g^{-1} in CNF0 to 0.59 and 0.88 mmol g^{-1} in CNF1 and CNF2, respectively.

Fig. 2a shows the XRD diffractograms of nanocellulose fibers, where cellulose I characteristic diffraction peaks can be seen at 15, 16.5, 23 and 34°, related to (101), (10$\bar{1}$), (002) and (040) crystallographic planes [28]. The obtained diffraction curves were deconvoluted by the Lorentz function (Fig. 2b), selecting the previously mentioned diffraction peaks, as well as a broad amorphous one at 21.5° [29]. Afterwards, the peaks were integrated in order to calculate their area. The crystallinity of nanocellulose fibers was calculated following the equation proposed by Hermans et al. (equation (1)) [30].

$$\text{C. I.}\,(\%) = \left(\frac{A_c}{A_c + A_a}\right) \times 100 \qquad (1)$$

where A_c and A_a are the areas related to the crystalline and amorphous peaks, respectively. The results obtained for crystallinity index are shown in Table 2.

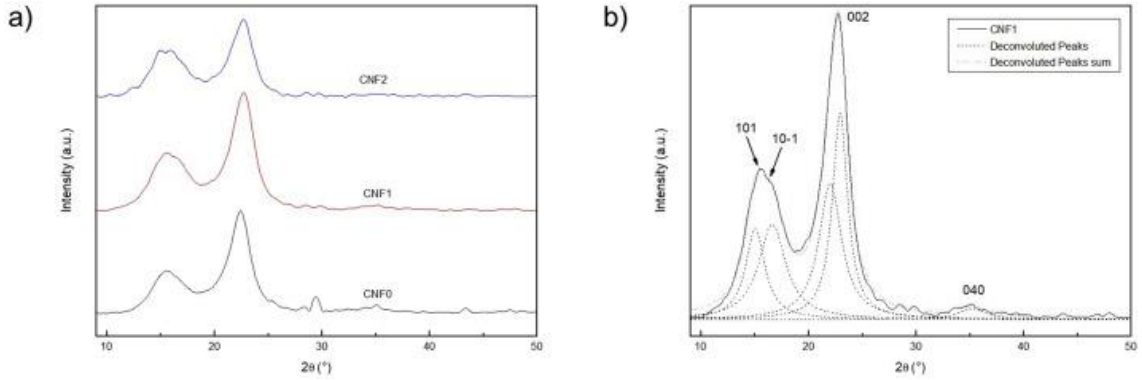

Fig.2. a) XRD diffractograms of cellulose nanofibers with different carboxylation degrees and b) deconvolution of peaks for CNF1 sample.

Table 2. Changes in crystallinity index for nanofibers with different carboxylation degrees.

Sample	C.I. (%)
CNF0	79
CNF1	68
CNF2	61

The results show that the undergone treatment, and the resulting increase of carboxyl group content, leads to a decrease in crystallinity for the nanofibers. The formation of new carboxyl groups, and thus the opening of the glucopyranose rings, entails damaging the ordered structure of the cellulose, making carboxylated cellulose nanofibers less crystalline [23,31].

The characteristic functional groups of cellulose nanofibers were studied by Fourier transform infrared spectroscopy and the obtained results are represented in Fig. 3. The absorption bands located at 3331 and 3375 cm^{-1} correspond to the stretching vibration of the OH groups, whereas the peak at 2900-2800 cm^{-1} is assigned to the C–H stretching vibration [32]. A band associated with the absorbed water is observed at 1635 cm^{-1} [33]. The band around 1429 cm^{-1} represents the symmetric bending of CH_2 [34]. The bands situated at 1160 and 897 cm^{-1} are attributed to C–O–C asymmetric stretching in β-glycosidic linkages, and the band at 1031 cm^{-1} to C–O stretching at C6 [32,[34], [35], [36]].

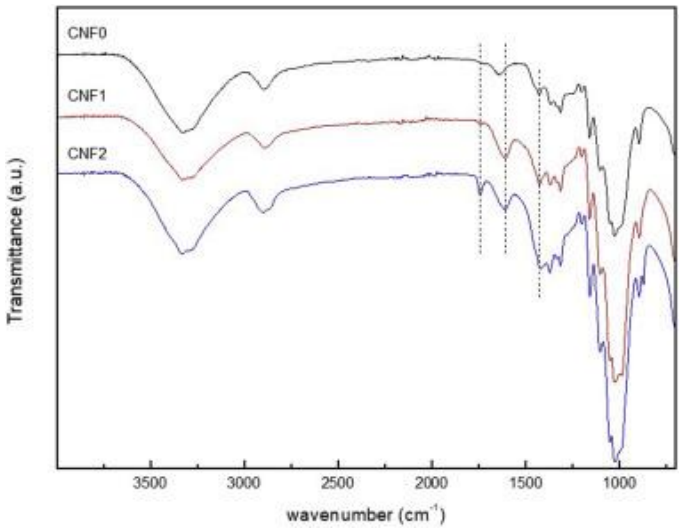

Fig. 3. FTIR spectra of cellulose nanofibers with different degrees of carboxylation.

Analyzing the carbonyl stretching vibration region of nanofiber carboxyl groups (denoted by dotted lines in Fig. 3), the different degrees of carboxylation of each sample can be seen. It is known from literature [37] that this band can vary easily with the effect of the humidity, temperature and pH. It tends to appear at 1735 cm^{-1} when protonated, whereas it displaces towards lower wavenumbers, around 1610 cm^{-1}, when it is in its salt form. Spectrum for CNF0 sample shows a small shoulder at 1735 cm^{-1}, whereas in the case of CNF1 and CNF2 samples, both bands, related to protonated and unprotonated carboxyl groups, are present. CNF1 spectrum maintains the shoulder at 1735 cm^{-1} and shows also a band at 1610 cm^{-1}, associated with both COONa groups and the overlapped absorbed water band. The spectrum for CNF2 sample presents the same behavior at 1610 cm^{-1}. However, it shows a distinguished band at 1742 cm^{-1}, suggesting a higher presence of COOH groups as well as COONa. Finally, the intensity of the band located

at 1430 cm^{-1} increases for CNF1 and CNF2 sample spectra, which is attributed to the formation of COONa [38].

As far as thermal stability is concerned, the resulting thermogravimetric curves are shown in Fig. 4 and the characteristic temperatures are reported in Table 3. All systems show an initial weight loss related to the water absorbed in the fibers. The derivative curve, i.e. DTG curve, for CNF0 sample presents a peak going from 220 to 390 °C, with a maximum at 346 °C, related to the degradation of cellulose crystalline domains. This peak starts at lower temperatures for both CNF1 and CNF2 fibers, and the maximum is also displaced to lower temperatures, 322 and 320 °C, respectively. This decrease in the onset degradation temperature, temperature at which a weight loss of 5 wt% takes place, could suggest that cellulose crystals are damaged after being modified, which is in agreement with X-ray results previously reported. Yue et al. also observed a decrease in the onset degradation temperature attributed to the rearranging process and changes in crystallinity that take place during the modification of the fibers [39]. Moreover, an intense shoulder can be seen at 230 °C for samples with higher carboxylation degrees, as has also been seen in previous studies of treated fibers [40], which has been attributed to their nanometric size the larger amount of free ends present.

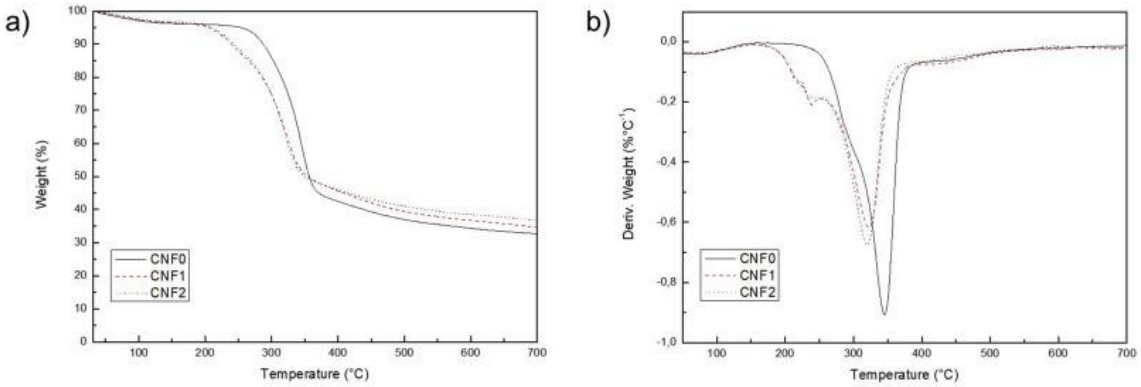

Fig. 4. a) TGA and b) DTG curves of cellulose nanofibers with different degrees of carboxylation.

Table 3. Thermal degradation behavior of cellulose nanofibers with different degrees of carboxylation.

Sample	T_{onset} (°C)	T_{Max} (°C)	Char Residue (%)
CNF0	282	346	34.3
CNF1	232	320	36.7
CNF2	233	322	38.5

In Table 3, both the degradation temperatures of the nanofibers and the remaining char after 600 °C are summarized. The observed difference in the remaining char of the different nanofibers could be due to the presence of carboxyl groups in the surface, which makes it more difficult to decompose them into smaller units [40]. Results show that the preparation method and the treatment of the fibers have great influence in the thermal properties of the resulting nanofibers.

3.2. WBPU dispersion characterization

The solid content of the synthesized WBPU was measured in triplicate by the weight difference between the dispersed and dried sample. The determined value was 31.40 ± 0.03 wt%, equal to the theoretical, denoting that all reagents were fully incorporated to the WBPU.

The particle size and distribution of the synthetized WBPU dispersion were analyzed by dynamic light scattering. The particle size is an important parameter when studying the stability of the WBPU dispersion. Dispersions with larger particle sizes tend to be less stable, due to the precipitation of these particles. On the other hand, dispersions with small particle sizes have better stability, thanks to the formation of thicker electrochemical double layer [3,41]. Results showed an average particle size of 178.2 ± 3.8 nm with a polydispersity of 0.023. The obtained results were similar to the ones reported in literature for stable WBPU dispersions [13]. Moreover, the particle size was also measured after 6 months, and did not change significantly, 184.3 ± 1.1 nm, denoting that the synthesized dispersion is stable for prolonged periods of time.

3.3. WBPU-CNF composite characterization

Composites films with different CNF systems were characterized in order to assess the effect that the content and the treatment of the fibers may have on the reinforced composites. It is expected that interactions between WBPU and cellulose nanofibers may be enhanced when carboxylated fibers are used. In addition to O–H groups, treated fibers count also with carboxylic groups in their surface, able to form hydrogen bonds with urethane groups of the polyurethane (Fig. 5).

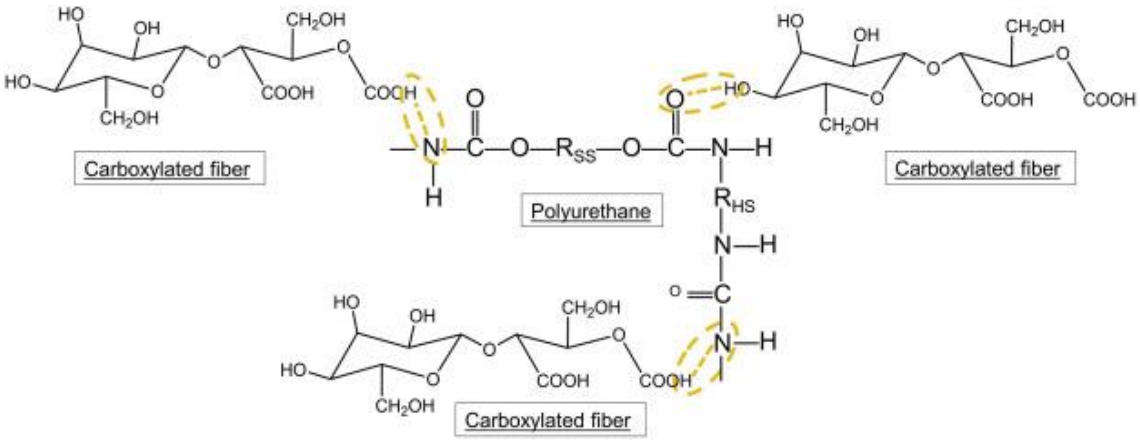

Fig. 5. Schematic representation of the interactions between WBPU and carboxylated CNF, where RSS refers to soft segment chain and RHS to hard segment chain.

Fig. 6 shows WBPU matrix and composite films reinforced with 5 wt% of cellulose nanofibers (3CNF0) and carboxylated cellulose nanofibers (3CNF1 and 3CNF2). Transparent films, with no significant differences between them, were obtained for all systems.

Fig. 6. Photographs of the prepared WBPU, 3CNF0, 3CNF1 and 3CNF2.

In order to assess a good dispersion of the nanofibers in the composites, SEM images of a cryofracture cross-section were obtained. Fig. 7a shows SEM image of WBPU matrix, whereas Fig. 7b–d show composites reinforced with a 3 wt% of CNF0, CNF1 and CNF2, where a good dispersion of the fibers can be observed, with no visible agglomerations. Fig. 7e shows SEM

image of 5CNF1 where, although a higher content of fibers can be seen, a homogenous dispersion of the fibers can still be observed.

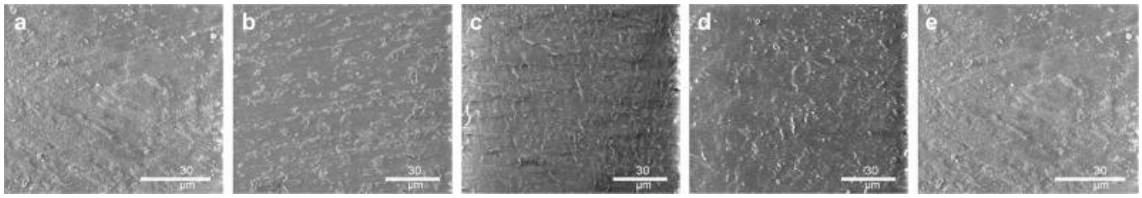

Fig. 7. SEM images for cryofracture of the cross-section of a) WBPU, b) 3CNF0, c) 3CNF1, d) 3CNF2 and e) 5CNF1.

The FTIR curve for the WBPU matrix (Fig. 8) shows an absorption band at 3369 cm^{-1}, which is assigned to hydrogen-bonded N–H groups of urethane and urea functional groups [42]. The band at 1731 cm^{-1} corresponds to the carbonyl vibration of the polyol and urethane groups [43], whereas the shoulder observed around 1645 cm^{-1} is attributed to carbonyl group stretching vibration of urea group [44]. The band situated at 1545 cm^{-1} in amide II region is assigned to the C–N stretching vibration and N–H bending of urethane and urea groups [3,45].

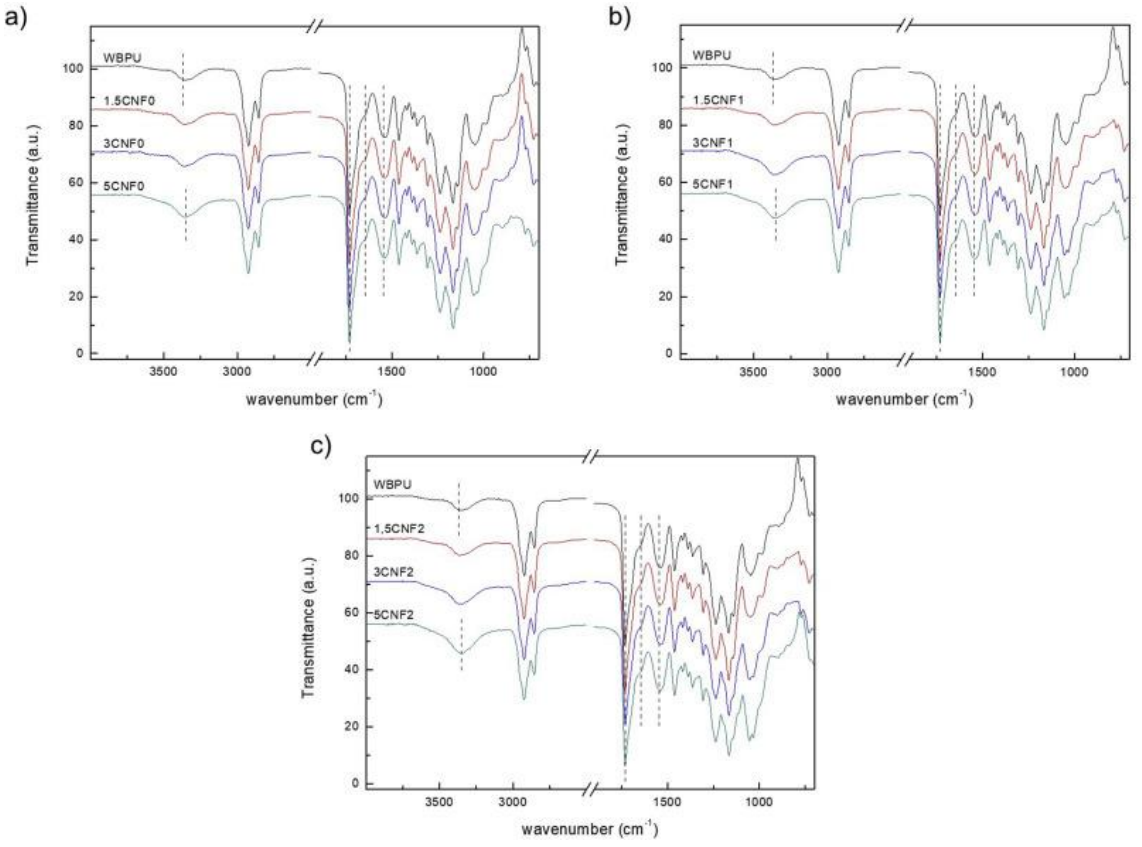

Fig. 8. FTIR spectra of neat WBPU and reinforced composites with different contents of: a) CNF0, b) CNF1 and c) CNF2.

Comparing the spectrum of the synthetized WBPU matrix with the spectra of the reinforced composites (Fig. 8 a-c), an increase in the intensity of the band located around 3300-3370 cm^{-1} is observed, which increases with the content of CNF. At the same time, for the composites with the highest CNF content, a slight shift of this band to lower wavenumber values can be observed (Fig. 8a–c). Changes in the stretching bond strength and length due to variation of chemical environment of the atoms involved in the bond can be seen more clearly in the second derivative curves, where the changes in wavenumber are seen by displacement of maximum peaks [46]. Fig.

9a shows a region (1200-1500 cm^{-1}) where no changes take place comparing the WBPU and reinforced composite spectra, i.e. without displacement of the maximum peaks. On the other hand, Fig. 9b shows the 3390-3320 cm^{-1} interval where hydrogen bonded interactions of N–H groups can be distinguished, as in the case of 5 CNF1 where the peaks shift to lower wavenumbers comparing with WBPU matrix. This fact could be related to the formation of new hydrogen bond interactions between matrix N–H and cellulose O–H groups.

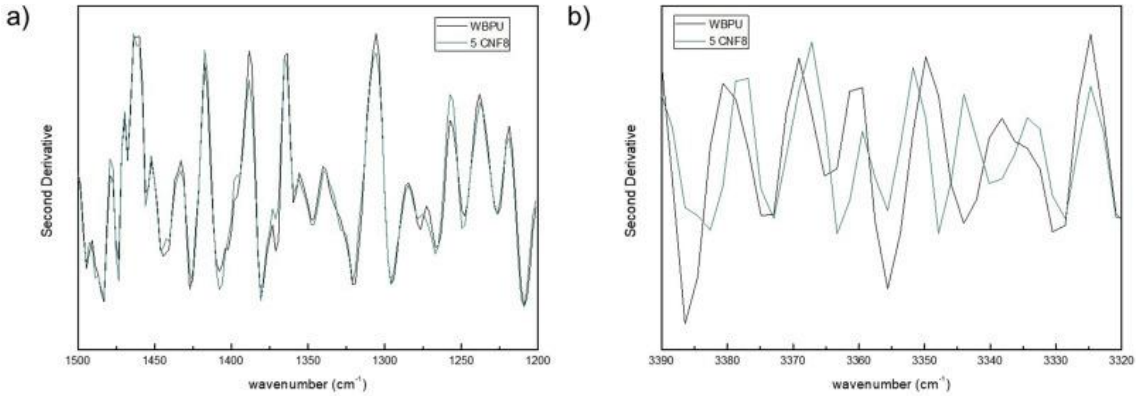

Fig. 9. Second derivative curves for WBPU and 5 CNF1 composite around a) 1500-1200 cm^{-1} and b) 3390-3320 cm^{-1}.

Thermal degradation of composites was studied by thermogravimetric analysis. The thermal degradation of polyurethanes takes places in two steps (Fig. 10). In the first step, the thermal degradation of the hard domain occurs, whereas in the second step degradation of soft segment takes place. Derivative curves show a peak around 330 °C with a shoulder around 265 °C related to the degradation of urethane and urea groups in the hard segment, respectively, and a second peak around 400 °C related to the degradation of the soft domain, mainly formed by the polyol [47].

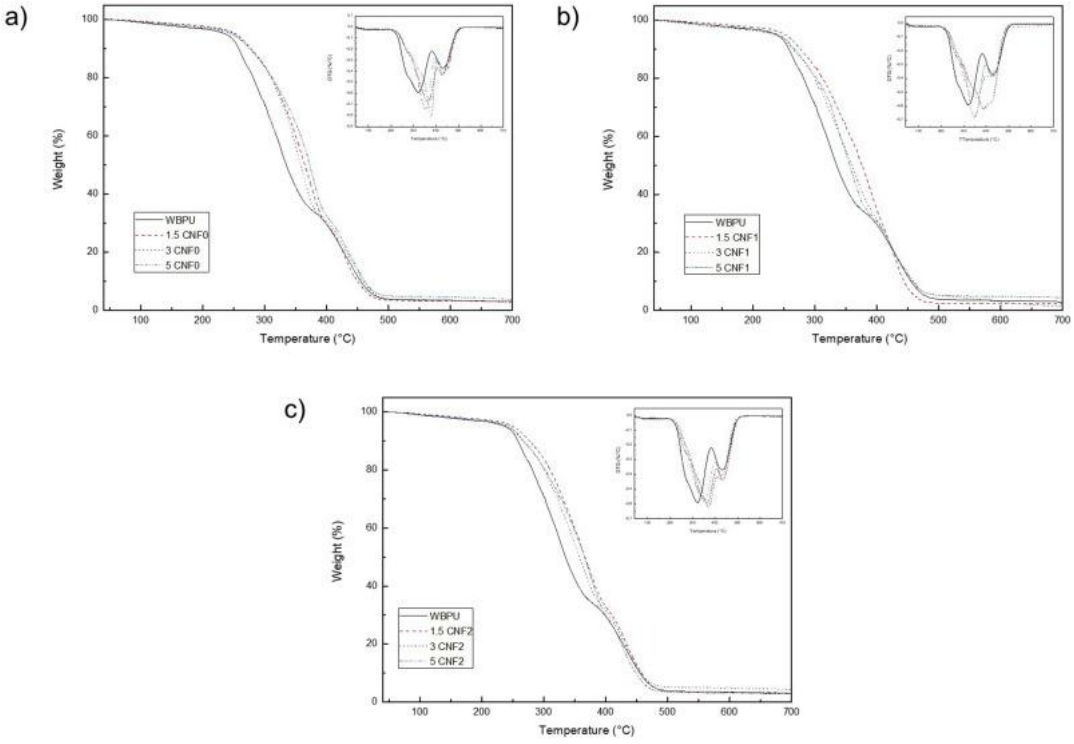

Fig. 10. Thermogravimetric analysis curves of WBPU matrix and reinforced composites with: a) CNF0, b) CNF1 and c) CNF2.

Regarding the thermal degradation of composites, it can be observed that it also occurs in two steps, but the weight loss related to hard domains shifts to higher temperatures, suggesting that the thermal stability of the composites is improved with the addition of CNFs. This improvement can be attributed to the interactions taking place between the CNFs and the WBPU, resulting in more stabilized urethane groups and more confined structures, thus enhancing the thermal stability of the materials, which is in agreement with other studies [48,49].

On the other hand, in order to analyze the thermal transitions of both WBPU matrix and composites, differential scanning calorimetry tests were performed. The obtained thermograms of the heating scan are represented in Fig. 11, and the values of endothermic transition attributed to short range ordering of the hard segment domains (T_{HS}) and soft segment glass transition (T_g) temperatures, as well as the relative short range ordering degrees (X_{HS}) are summarized in Table 4. The relative short range ordering degree of the composites was calculated following equation (2), proposed by Wunderlich [50].

$$X_{HS} = \frac{\Delta H_{HS_c}}{w \cdot \Delta H_{HS}} \cdot 100 \qquad (2)$$

where ΔH_{HSc} represents the measured enthalpy of the composite transition, whereas ΔH_{HS} is related to the measured enthalpy of the polyurethane matrix short range ordering transition and w is the weight fraction of the WBPU in the composite.

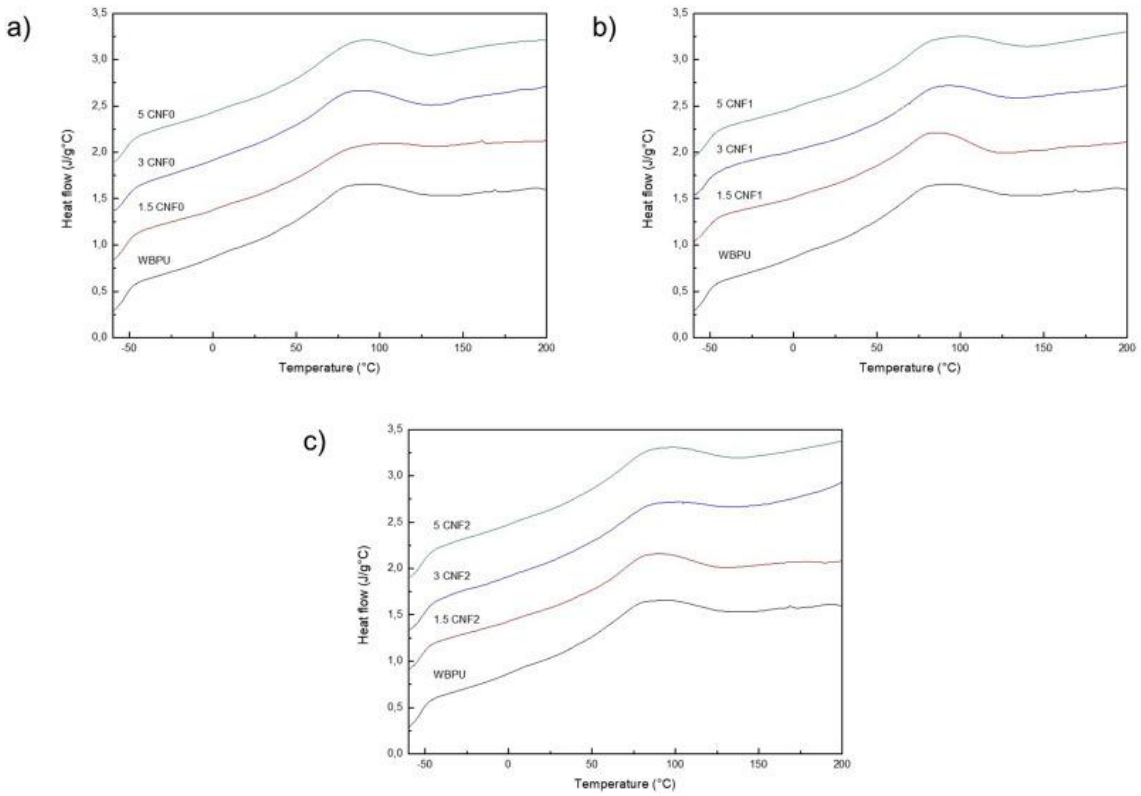

Fig. 11. DSC curves of WBPU matrix and reinforced composites with different contents of: a) CNF0, b) CNF1 and c) CNF2.

Although the soft segment glass transition temperature remains nearly constant, the short range ordering transition temperatures and their enthalpies increase with the addition of CNFs, and therefore so does the relative short range ordering degree of the composites, which might suggest interactions between the matrix and the nanofibers, as previously observed by FTIR and agreeing with TGA results. The new assembling in the materials hinders the disruption of the short range ordered structures of the composite. With the addition of low quantities of CNFs, a significant

increase in the relative short range ordering degree of the composites is observed, such as in the case of 1.5 wt% CNF where a 17% increase is achieved for CNF0, going up to 37% for fibers with higher degree of carboxylation.

Table 4. Values of different thermal transitions observed from the DSC curves.

Sample	T_g (°C)	T_{HS} (°C)	ΔH_{HSc} (J/g)	X_{HS} (%)
WBPU	−52.0	81.4	10.5	100
1.5 CNF0	−52.9	83.2	12.4	117
3 CNF0	−53.2	81.9	13.9	132
5 CNF0	−52.6	85.7	15.0	142
1.5 CNF1	−51.3	81.9	14.1	133
3 CNF1	−53.9	86.1	15.0	142
5 CNF1	−52.3	85.1	17.4	165
1.5 CNF2	−53.2	82.4	14.4	137
3 CNF2	−52.5	85.4	15.8	150
5 CNF2	−51.9	86.1	16.8	159

At the same reinforcement content, carboxylation seems to improve the interactions between the matrix and the fibers, resulting in composites with higher degree of short range ordering.

The influence of cellulose nanofibers on the thermomechanical behavior of the materials was also studied by dynamic mechanical tests. Fig. 12 shows the temperature dependence of the storage modulus (E') and loss factor (tan δ) for the WBPU matrix and composites. The storage modulus curves show a similar behavior for all the composites in the glassy state up to around −45 °C, where a drop, and simultaneously a maximum peak in tan δ curve can be observed, which is related to the T_g of the soft segment, also seen by DSC. From that transition on, in the rubbery state, the storage modulus curve of the matrix continues decreasing, whereas the reinforced systems show a more gradual decrease, resulting in composites with higher thermomechanical stability. The composites with the highest amount of CNFs are the ones with higher and more stable modulus values, suggesting thus the effective reinforcement effect of CNFs. Regarding the effect of carboxylation degree, composites prepared with either CNF1 and CNF2 showed higher modulus values above T_g than CNF0. The addition of CNFs also results in materials with more interactions and higher ordering degrees as observed by DSC, which also translates into materials with higher thermomechanical stability.

This effect can also be seen in the maximum of tan δ curves. The tan δ peak damping is bigger for the WBPU matrix than for the composites. Moreover, damping decreased with increasing CNF content. This may be due to the interactions between the matrix and the fibers, which hampers the mobility of the WBPU chains [51]. For reinforced materials, a second transition peak is also present at around 50 °C in tan δ curves. This transition is attributed to the breaking of the short rang ordering of the hard segment domains, which is in agreement with DSC data reported

previously. The presence of cellulose nanofibers on the systems supplies a higher structural integrity to the composites, impeding the materials from flowing, and thus this peak can be seen for composite films.

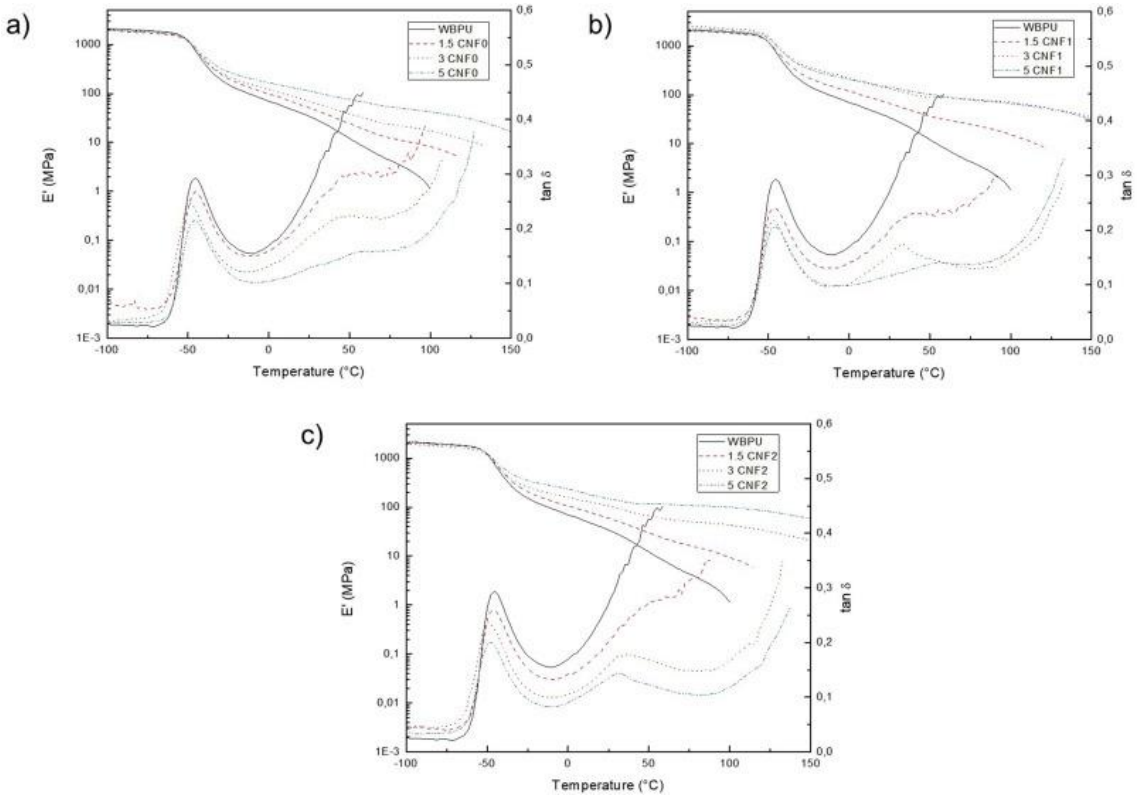

Fig. 12. Dynamic-mechanical curves of neat WBPU matrix and reinforced composites with different contents of: a) CNF0, b) CNF1 and c) CNF2.

The mechanical properties of the WBPU matrix are also significantly altered with the addition of CNFs as it can be observed by the results obtained by tensile tests (Fig. 13). In order to consider the significance of the undertaken changes on the composites, analysis of variance (ANOVA) was carried out. Anova was conducted with OriginPro8 (Origin Lab), using the Turkey's test at a significant level of 0.05. Results are represented on Fig. 13, being the systems that do not share any letters significantly different.

As can be observed in the results, the addition of cellulose nanofibers to the waterborne polyurethane matrix results in a significant improvement of the Young modulus values (Fig. 13a), which could be attributed to the increase in relative short range ordering degree of the composites and the reinforcement effect of CNFs. These results are similar to the ones reported by different authors [52], proving the good interaction of both components of the composites. Comparing composites prepared with the same CNF content, only at 5 wt% of nanofibers significant differences could be observed, the highest Young's modulus is observed for the composite with CNF1, which is in correlation with the properties observed for neat CNF1 fiber and the short range ordering degree observed by DSC for the composite.

Regarding the stress at yield and stress at break, the addition of CNFs results in an increase of these values, even for small CNF contents. These changes are more significant for stress at yield values, where an increase of over 60% is achieved for all composites prepared with just 1.5 wt% of CNFs. In the case of stress at break, most systems show differences from the matrix but remain at similar values among them. Despite nanocomposites prepared with 5 wt% of CNFs showing higher stress at break values than the matrix, this values are lower than the values obtained for

their homologues with lower CNF contents, which suggests the presence of agglomerates in the composites prepared with high CNF content. This was also observed by other authors at high reinforcement contents [53]. The increase observed for stress at yield and stress at break values could be due to the effective stress transfer between the matrix and the reinforcement.

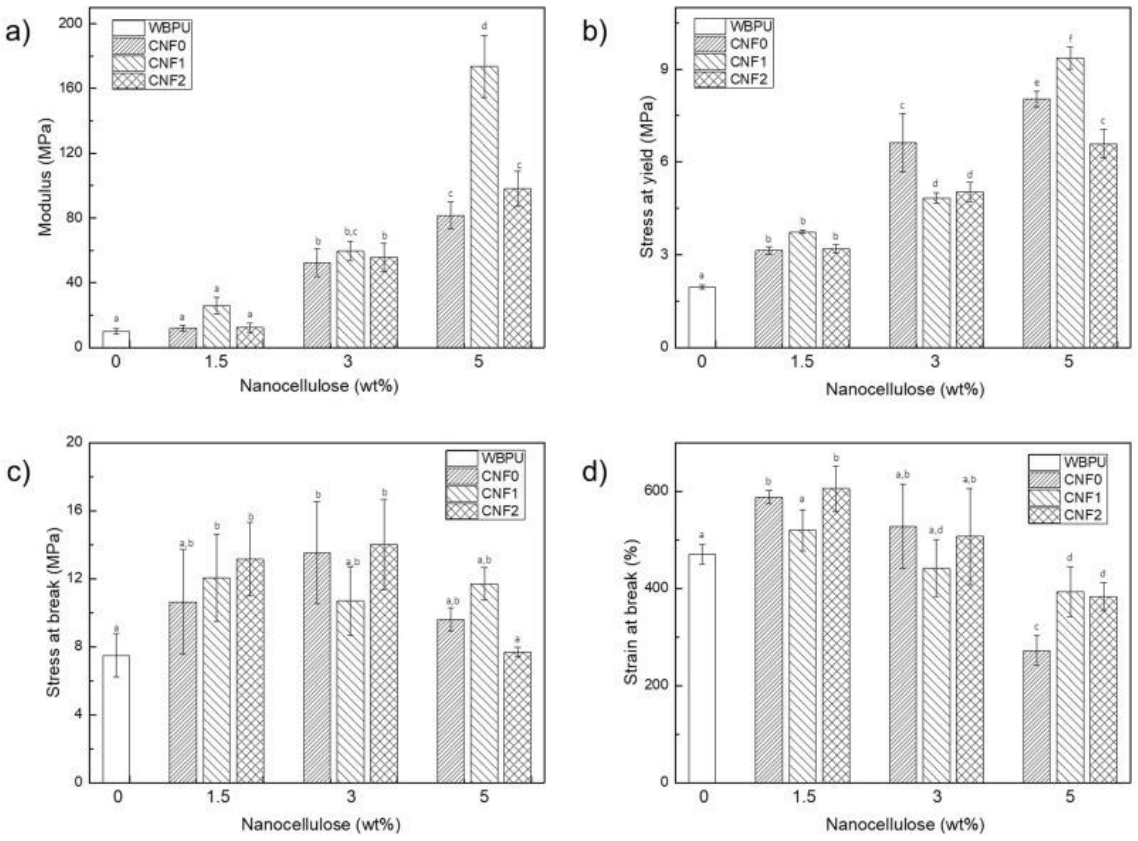

Fig. 13. a) Young modulus, b) Stress at yield, c) Stress at break and d) Strain at break values, for neat polymer and reinforced composites. Values analyzed using one-way ANOVA with Tukey's test, different letters indicate statistical differences.

Finally, when assessing the strain at break, composites with low CNF contents show similar values to neat WBPU. Although most studies found in the literature show a decrease in strain to failure from the matrix, due to an interfacial debonding which grows into a crack in the material [49,54,55], there are also some works where strain to failure values are maintained [45,48,56], modulated by reinforcement aspect ratio and matrix-reinforcement interaction, resulting in overall mechanically improved composites. The lower strain to failure values obtained for the composites prepared with 5 wt% of CNFs could be due to the presence of agglomerations as previously suggested.

Analyzing the results, it can be concluded that both content and type of cellulose have a significant effect of the mechanical properties of the composites. Behavioral changes are more statistically significant in the case of modulus and stress at yield.

4. Conclusion

In this work, cellulose nanofibers with different degrees of carboxylation have been prepared and used as reinforcements to prepare nanocomposites. A stable waterborne polyurethane dispersion has been synthetized and used as matrix. The effect of carboxylation and its degree have been studied on both the fibers and the composites final properties.

The results suggest the formation of interactions between the polymeric matrix and the reinforcements, showing an improvement in the general properties of the composites with the addition of CNFs. Although composites present the same degradation trend as the neat matrix, the thermal stability of waterborne polyurethane matrices have been improved with the addition of CNFs. A clear increase in the short range ordering degree of the composites takes place with the addition of cellulose nanofibers, due to the formation of new interactions between cellulose and polyurethane matrix. The thermomechanical stability of the films has been improved with the addition of CNFs, as well as the mechanical properties, being this improvement proportional to the amount of CNF added.

Lastly, it has been observed that the carboxylic groups at the fibers surface promote interactions within the system. However, an excess amount of carboxylic groups seems to damage nanocellulose crystal structure, thus affecting the final properties of the composites.

Declaration of competing interest

The authors declare that they have no known competing financial interests or personal relationships that could have appeared to influence the work reported in this paper.

Acknowledgements

Financial support from Basque Government (Grupos Con- solidados IT776-13 and ELKARTEK (KK-2016/00043)), University of the Basque Country (GIU18-216 research group), Spanish Ministry of Economy, Industry and Competitiveness (MAT2016-76294-R) is acknowledged. We also wish to acknowledge the “Macrobehavior- Mesostructure-Nanotechnology” SGIker unit from the University of the Basque Country, for their technical support. I. L. thanks Basque Government for PhD Fellowship (PRE_2017_1_0085).

References

[1] UNFCCC, Conference of the Parties (COP), Adoption of the paris agreement, in: Proposal by the President., Paris Clim. Chang. Conf. - Novemb. 2015, COP, vol. 21, 2015, p. 32, 21932.

[2] J. Hu, K. Peng, J. Guo, D. Shan, G.B. Kim, Q. Li, E. Gerhard, L. Zhu, W. Tu, W. Lv, M.A. Hickner, J. Yang, Click cross-linking-improved waterborne polymers for environment-friendly coatings and adhesives, ACS Appl. Mater. Interfaces 8 (2016) 17499e17510, https://doi.org/10.1021/acsami.6b02131.

[3] A. Santamaria-Echart, A. Arbelaiz, A. Saralegi, B. Fern´andez-d’Arlas, A. Eceiza, M.A. Corcuera, Relationship between reagents molar ratio and dispersion stability and film properties of waterborne polyurethanes, Colloids Surfaces A Physicochem. Eng. Asp. 482 (2015) 554e561, https://doi.org/10.1016/ j.colsurfa.2015.07.012.

[4] PlasticsEurope, Plastics e the Facts 2017. An Analysis of European Plastics Production, Demand and Waste Data, 2017.

[5] PlasticsEurope, World plastics materials demand 2015, Plast. Mark. Res. Gr./ Consult. Mark. Ind. GmbH (2016) 3.

[6] H. Honarkar, Waterborne polyurethanes: a review, J. Dispersion Sci. Technol. 2691 (2017) 1e10.

[7] M. Tharcis, T. Badel, S. Je´ol, E. Fleury, F. Me´chin, High elongation thermoplastic Polyester-urethanes based on widely available diacid intermediates, J. Appl. Polym. Sci. 133 (2016) 1e15.

[8] S.A. Madbouly, Y. Xia, M.R. Kessler, Rheological behavior of environmentally friendly castor oil-based waterborne polyurethane dispersions, Macromole- cules 46 (2013) 4606e4616, https://doi.org/10.1021/ma400200y.

[9] Y. Lu, R.C. Larock, Soybean-oil-based waterborne polyurethane dispersions: effects of polyol functionality and hard segment content on properties, Bio- macromolecules 9 (2008) 3332e3340, https://doi.org/10.1021/bm801030g.

[10] G. Çaylı, S. Küsefogˇlu, Biobased polyisocyanates from plant oil triglycerides: synthesis, polymerization, and characterization, J. Appl. Polym. Sci. 109 (2008) 2948e2955.

[11] L. Hojabri, X. Kong, S.S. Narine, Fatty Acid-Derived diisocyanate and biobased polyurethane produced from vegetable oil: synthesis, polymerization, and characterization, Biomacromolecules 10 (2009) 884e891.

[12] H. Khatoon, S. Ahmad, A review on conducting polymer reinforced poly- urethane composites, J. Ind. Eng. Chem. 53 (2017) 1e22.

[13] A. Santamaria-Echart, L. Ugarte, C. García-Astrain, A. Arbelaiz, M.A. Corcuera, A. Eceiza, Cellulose nanocrystals reinforced environmentally-friendly water- borne polyurethane nanocomposites, Carbohydr. Polym. 151 (2016) 1203e1209.

[14] L. Wang, M. Ando, M. Kubota, S. Ishihara, Y. Hikima, M. Ohshima, T. Sekiguchi, A. Sato, H. Yano, Effects of hydrophobic-modified cellulose nanofibers (CNFs) on cell morphology and mechanical properties of high void fraction poly- propylene nanocomposite foams, Compos. Part A Appl. Sci. Manuf. 98 (2017) 166e173.

[15] A.K. Barick, D.K. Tripathy, Effect of nanofiber on material properties of vapor- grown carbon nanofiber reinforced thermoplastic polyurethane (TPU/CNF) nanocomposites prepared by melt compounding, Compos. Part A Appl. Sci. Manuf. 41 (2010) 1471e1482.

[16] C. Castro, A. Vesterinen, R. Zuluaga, G. Caro, I. Filpponen, O.J. Rojas, G. Kortaberria, P. Gan~a´n, In situ production of nanocomposites of poly(vinyl alcohol) and cellulose nanofibrils from Gluconacetobacter bacteria: effect of chemical crosslinking, Cellulose 21 (2014) 1745e1756.

[17] R.J. Moon, G.T. Schueneman, J. Simonsen, Overview of cellulose nanomaterials, their capabilities and applications, JOM (J. Occup. Med.) 68 (2016) 2383e2394.

[18] V. Zˇepiˇc, I. Poljanˇsek, P. Oven, M. Cˇop, COST-FP1105: Properties of PLA Films Reinforced with Unmodified and Acetylated Freeze Dried Nanofibrillated Cellulose, 2016.

[19] Y. Habibi, Key advances in the chemical modification of nanocelluloses, Chem. Soc. Rev. 43 (2014) 1519e1542.

[20] S. Eyley, W. Thielemans, Surface modification of cellulose nanocrystals, Nanoscale 6 (2014) 7764e7779.

[21] A. Isogai, T. Saito, H. Fukuzumi, TEMPO-oxidized cellulose nanofibers, Nano- scale 3 (2011) 71e85.

[22] H. Yang, A. Tejado, N. Alam, M. Antal, T.G.M. Van De Ven, Films prepared from electrosterically stabilized nanocrystalline cellulose, Langmuir 28 (2012) 7834e7842.

[23] U.-J. Kim, S. Kuga, M. Wada, T. Okano, T. Kondo, Periodate oxidation of crys- talline cellulose, Biomacromolecules 1 (2000) 488e492.

[24] K. Hua, I. Rocha, P. Zhang, S. Gustafsson, M. Stromme, A. Mihranyan, N. Ferraz, Transition from Bioinert to Bioactive Material by Tailoring the Biological Cell Response to Carboxylated Nanocellulose Transition from Bioinert to Bioactive Material by Tailoring the Biological Cell Response to Carboxylated Nano- cellulose, 2016, https://doi.org/10.1021/acs.biomac.6b00053.

[25] D. Cheng, Y. Wen, X. An, X. Zhu, Y. Ni, TEMPO-oxidized cellulose nanofibers (TOCNs) as a green reinforcement for waterborne polyurethane coating (WPU) on wood, Carbohydr, Polymers 151 (2016) 326e334.

[26] A. Tejado, M.N. Alam, M. Antal, H. Yang, T.G.M. van de Ven, Energy re- quirements for the disintegration of cellulose fibers into cellulose nanofibers, Cellulose 19 (2012) 831e842.

[27] M.N. Alam, M. Antal, A. Tejado, T.G.M. van de Ven, Salt-induced acceleration of chemical reactions in cellulose nanopores, Cellulose 19 (2012) 517e522.

[28] J. He, S. Cui, S. Wang, Preparation and crystalline analysis of high-grade bamboo dissolving pulp for cellulose acetate, J. Appl. Polym. Sci. 107 (2008) 1029e1038.

[29] S. Park, J.O. Baker, M.E. Himmel, P.A. Parilla, D.K. Johnson, Cellulose crystal- linity index: measurement techniques and their impact on interpreting cellulase performance, Biotechnol. Biofuels 3 (2010) 1e10.

[30] P.H. Hermans, A. Weidinger, Quantitative X-ray investigations on the crys- tallinity of cellulose fibers. A background analysis, J. Appl. Phys. 19 (1948) 491e506.

[31] Q.X. Hou, W. Liu, Z.H. Liu, L.L. Bai, Characteristics of wood cellulose fibers treated with periodate and bisulfite, Ind. Eng. Chem. Res. 46 (2007) 7830e7837.

[32] J. Sˇiroký, R.S. Blackburn, T. Bechtold, J. Taylor, P. White, Attenuated total reflectance Fourier-transform Infrared spectroscopy analysis of crystallinity changes in lyocell following continuous treatment with sodium hydroxide, Cellulose 17 (2010) 103e115.

[33] M. Sain, S. Panthapulakkal, Bioprocess preparation of wheat straw fibers and their characterization, Ind. Crop. Prod. 23 (2006) 1e8.

[34] M. Jonoobi, J. Harun, A. Shakeri, M. Misra, K. Oksmand, Chemical composition, crystallinity, and thermal degradation of bleached and unbleached kenaf bast (Hibiscus cannabinus) pulp and nanofibers, BioResources 4 (2009) 626e639.

[35] J.G. Gwon, S.Y. Lee, G.H. Doh, J.H. Kim, Characterization of chemically modified wood fibers using FTIR spectroscopy for biocomposites, J. Appl. Polym. Sci. 21 (2010). NA-NA.

[36] G. Mondragon, S. Fernandes, A. Retegi, C. Pen~a, I. Algar, A. Eceiza, A. Arbelaiz,A common strategy to extracting cellulose nanoentities from different plants, Ind. Crop. Prod. 55 (2014) 140e148.

[37] R.G. Zhbankov, Infrared Spectra of Cellulose and its Derivatives, Springer US, Boston, MA, 1995.

[38] L.J. Bellamy, The Infra-red Spectra of Complex Molecules, Springer Netherlands, Dordrecht, 1975.

[39] Y. Yue, G. Han, Q. Wu, Transitional properties of cotton fibers from cellulose i to cellulose II structure, BioResources 8 (2013) 6460e6471.

[40] B. Soni, E.B. Hassan, B. Mahmoud, Chemical isolation and characterization of different cellulose nanofibers from cotton stalks, Carbohydr. Polym. 134 (2015) 581e589.

[41] S.K. Gaddam, A. Palanisamy, Anionic waterborne polyurethane dispersions from maleated cotton seed oil polyol carrying ionisable groups, Colloid Polym. Sci. 294 (2016) 347e355.

[42] I. Yilgo€r, E. Yilgo€r, G.L. Wilkes, Critical parameters in designing segmented polyurethanes and their effect on morphology and properties: a compre- hensive review, Polymers 58 (2015). A1eA36.

[43] L. Ugarte, B. Ferna´ndez-d'Arlas, A. Valea, M.L. Gonza´lez, M.A. Corcuera, A. Eceiza, Morphology-properties relationship in high-renewable content polyurethanes, Polym. Eng. Sci. 54 (2014) 2282e2291, https://doi.org/ 10.1002/pen.23777.

[44] A. Santamaria-Echart, I. Fernandes, A. Saralegi, M.R.P.F.N. Costa, F. Barreiro, M.A. Corcuera, A. Eceiza, Synthesis of waterborne polyurethane-urea disper- sions with chain extension step in homogeneous and heterogeneous media, J. Colloid Interface Sci. 476 (2016) 184e192, https://doi.org/10.1016/ j.jcis.2016.05.016.

[45] A. Pei, J.M. Malho, J. Ruokolainen, Q. Zhou, L.A. Berglund, Strong nano- composite reinforcement effects in polyurethane elastomer with low volume fraction of cellulose nanocrystals, Macromolecules 44 (2011) 4422e4427, https://doi.org/10.1021/ma200318k.

[46] A. Orue, A. Santamaria-Echart, A. Eceiza, C. Pen~a-Rodriguez, A. Arbelaiz, Office waste paper as cellulose nanocrystal source, J. Appl. Polym. Sci. 134 (2017) 1e11.

[47] C.W. Ou, C.H. Su, U.S. Jeng, S.H. Hsu, Characterization of biodegradable poly- urethane nanoparticles and thermally induced self-assembly in water dispersion, ACS Appl. Mater. Interfaces 6 (2014) 5685e5694, https://doi.org/ 10.1021/am500213t.

[48] A. Santamaria-Echart, L. Ugarte, A. Arbelaiz, N. Gabilondo, M.A. Corcuera, A. Eceiza, Two different incorporation routes of cellulose nanocrystals in waterborne polyurethane nanocomposites, Eur. Polym. J. 76 (2016) 99e109.

[49] X. Cao, Y. Habibi, L.A. Lucia, One-pot Polymerization , Surface Grafting , and Processing of Waterborne Polyurethane-Cellulose Nanocrystal Nano- composites, 2009, pp. 7137e7145, https://doi.org/10.1039/b910517d.

[50] B. Wunderlich, Thermal Analysis of Polymeric Materials, 2005.

[51] B. Ly, W. Thielemans, A. Dufresne, D. Chaussy, M.N. Belgacem, Surface func- tionalization of cellulose fibres and their incorporation in renewable poly- meric matrices, Compos. Sci. Technol. 68 (2008) 3193e3201.

[52] M.L. Auad, V.S. Contos, S. Nutt, M.I. Aranguren, N.E. Marcovich, Characteriza- tion of nanocellulose- reinforced shape memory polyurethanes, Polym. Int. 57 (2008) 651e659.

[53] G.A. Jimenez, S.C. Jana, Composites of carbon nanofibers and thermoplastic polyurethanes with shape-memory properties prepared by chaotic mixing, Polym. Eng. Sci. 49 (2009) 2020e2030.

[54] X. Cao, H. Dong, C.M. Li, New nanocomposite materials reinforced with flax cellulose nanocrystals in waterborne polyurethane, Biomacromolecules 8 (2007) 899e904, https://doi.org/10.1021/bm0610368.

[55] G. Mondragon, A. Santamaria-Echart, M.E.V. Hormaiztegui, A. Arbelaiz, C. Peña-Rodriguez, V. Mucci, M. Corcuera, M.I. Aranguren, A. Eceiza, Nano- composites of waterborne polyurethane reinforced with cellulose nano- crystals from sisal fibres, J. Polym. Environ. (2017) 1e12, 0.

[56] A. Santamaria-Echart, I. Fernandes, L. Ugarte, F. Barreiro, A. Arbelaiz, M.A. Corcuera, A. Eceiza, Waterborne polyurethane-urea dispersion with chain extension step in homogeneous medium reinforced with cellulose nanocrystals, Compos. B Eng. 137 (2018) 31e38, https://doi.org/10.1016/ j.compositesb.2017.11.004.